Available online at www.sciencedirect.com
SCIENCE DIRECT®
ELSEVIER
Nuclear Instruments and Methods in Physics Research B 231 (2005) 292–299
NIM B
Beam Interactions with Materials & Atoms
www.elsevier.com/locate/nimb

Skin morphology and layer identification using different STIM geometries

P. Aguer [a], L.C. Alves [b], Ph. Barberet [a], E. Gontier [a], S. Incerti [a], C. Michelet-Habchi [a], Zs. Kertész [c], A.Z. Kiss [c], P. Moretto [a], J. Pallon [d], T. Pinheiro [b,*], J.E. Surlève-Bazeille [e], Z. Szikszai [c], A. Veríssimo [b], M.D. Ynsa [a]

[a] *CENBG-IN2P3/CNRS, BP120, 33175 Gradignan cedex, France*
[b] *Laboratório de Feixes de Iões, Instituto Tecnológico e Nuclear, Sacavém, Portugal and Centro de Física Nuclear, Universidade de Lisboa, Portugal*
[c] *Institute of Nuclear Research/ATOMKI/Debrecen, Pf. 51, H-4001, Hungary*
[d] *Lund Institute of Technology, Physics Department, Lund University, Sweden*
[e] *DMPFCS, Université Bordeaux 1, Talence, France*

Available online 23 March 2005

Abstract

The use of on-axis geometry in scanning transmission ion microscopy (STIM) has been widely used for thin biological sample structure identification. In this configuration, the lateral resolution is optimised so that micron or submicron beam spots are easily achieved even for classic microbeam lines. Off-axis STIM was more particularly employed for rapid imaging, and also (when associated to a scattering set-up) for normalising elemental contents obtained by other ion beam analysis techniques in organic thin samples. Due to the very small beam current required, on-axis STIM is a stand-alone technique. Off-axis STIM can be advantageous as it enables the simultaneous utilisation of PIXE and RBS techniques. In this paper, the STIM images obtained with an on-axis geometry, a standard off-axis geometry and a recently developed on–off geometry are presented and discussed. Data from skin samples are used for comparison purposes aiming at studying skin permeability to sunscreens. Skin is a stratified tissue and the precise identification of skin layers is needed to ascertain the penetration depth of the physical filter from the formulation. In addition to the intrinsic difference in image quality due to the beam resolution, the influence of the detector type, implanted silicon detector versus Si pin diode, is discussed on the basis of their energy resolution, their resistance to beam damage as well as the effect

* Corresponding author. Tel.: +351 219 946 250; fax: +351 219 941 525.
E-mail address: murmur@itn.pt (T. Pinheiro).

0168-583X/$ - see front matter
doi:10.1016/j.nimb.2005.01.073

of the sample thickness in the final image obtained. Data reduction software is also presented for the different geometries and the effect of parameters such as median or mean energy on the image quality is shown.

PACS: 87.59.Jq; 87.57.Ce; 07.05.Rm; 07.79.−v

Keywords: STIM; Beam damage; Image quality

1. Introduction

Topical sunscreens containing micronised particles (<50 nm) of titanium dioxide (TiO_2) have become essential in providing protection to human skin by its ability to scatter UV wavelengths of sunlight [1].

Although formulations containing TiO_2 are widely used, the transepidermic penetration and clearance of such particles is largely unknown. Also the role of TiO_2 particles when irradiated by UV light in oxygen free radical formation and/or magnification of UV-induced skin damage is far from being clarified [2]. Some of these questions are addressed by a EU funded project NANODERM, where nuclear microprobe analysis will be applied to assess the skin penetrability of TiO_2 particles dispersed in sunscreen products. High contrast STIM images in combination with Ti profile carried out by PIXE along skin layers is fundamental to validate whether TiO_2 particles reach the first line of living cells of the stratified epidermis in exposed skin.

In this work, three different geometries for STIM analysis are presented and their advantages and drawbacks in the analysis of thin biological tissues discussed. In particular, the applicability of STIM technique in skin permeability studies will be presented. Quality of the obtained STIM images is also discussed in terms of detector type and radiation damage hardness, data reduction method and sample preparation.

2. Material and methods

2.1. Skin sample preparation

Samples of mouse foot sole, pig and human skin were used in the study. Skin was collected by punch biopsy (3 mm minimum diameter), immediately frozen in 2-methylbutane cooled in LN_2 and kept in appropriated containers until processing at −70 °C or in LN_2 containers. Sections of 14 μm and 20 μm thickness were done in a cryostat at −25 °C, allowed to dry inside the cryostat and mounted in specific frames in self-supported mode hold by the edges with carbon tape.

2.2. Experimental

The general description of the nuclear microprobe set-ups available at the Bordeaux, Debrecen, Lisbon and Lund centres can be found elsewhere [3–6]. Therefore, only the different systems used for STIM analysis will be discussed in this paper.

Basic equipment components to perform STIM analysis consists of a particle detector coupled to typical electronic modules. STIM analysis may however differ in the type of experimental geometry and on the choice of the particle detector. The different STIM geometries used in this work are schematised in Fig. 1, and their advantages and drawbacks presented in the following sections.

2.2.1. On-axis STIM

This type of geometry is characterized by the location of the particle detector at 0° with the beam, at a certain distance behind the sample. At Bordeaux a 25 mm^2 PIPS detector is located just behind the sample implying a very large acceptance solid angle (almost 2π). The system at Debrecen also uses a 50 mm^2 PIPS detector at 60 mm from the sample although a large area PIN diode (Hamamatsu S3590-02) has also been tested. The system at Lisbon uses a 3×3 mm^2 Hamamatsu S1233-01 PIN diode with a 2.5 mm diameter collimator located at 40 mm from the sample that leads to an acceptance half-angle of 1.8°. A large

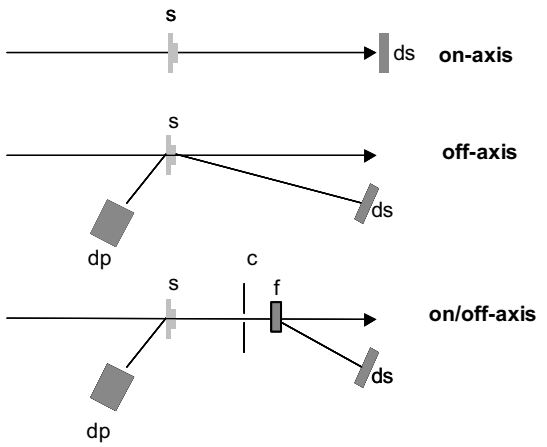

Fig. 1. Schematised STIM geometries. dp – PIXE detector, ds – STIM detector, s – sample, c – collimator, f – scattering foil.

acceptance angle assures that the number of particles detected is almost the same for every pixel, thus preserving counting statistics independent on the crossed sample thickness. Systems with smaller acceptance angle may receive different number of particles per pixel when different sample thickness is crossed due to a larger lateral beam straggling. This may increase uncertainty when statistical data treatment is used for map generation. The beam currents required for on-axis STIM analysis are very low (100–5000 ions/s) and therefore it is a stand-alone technique.

2.2.2. Off-axis STIM

Using a scattering angle between 15° and 45°, STIM can be performed in a so called off-axis mode providing the simultaneous use of PIXE and RBS techniques while maintaining some capabilities for sample features identification. At the Lisbon set-up, the PIN diode is coupled to a rotating flange that allows it to be wound into the beam axis or out of it, to an angle of 25°, while at Debrecen although usually on-axis STIM is used, an off-axis geometry created by covering the middle of the PIPS detector was tested. Usually, only STIM on-axis is performed at Bordeaux.

2.2.3. On/off-axis STIM

The on/off-axis STIM is a modified version of the off-axis STIM geometry that was developed and is used by the Lund group. This geometry includes a small collimator followed by a thin (40 μg/cm^2) carbon foil located ~3 cm from the sample that scatters the beam into a particle detector [7]. This system guarantees that the beam scattered in the sample does not reach the detector and that only beam with electronic energy loss is accepted at the thin monoelemental scattering foil. This assures that only information of the real sample cross-section is obtained. Simultaneous use of PIXE and RBS techniques is possible.

3. Image quality dependence

3.1. STIM geometry

The low beam current used in on-axis STIM is obtained by having a tiny aperture of both object and collimation slits, resulting in a high spatial beam resolution where sub-micron values are usually obtained. This geometry then provides the best possible image contrast of the sample mass density.

Opening the object and/or the collimation slits for obtaining beam currents above 100 pA, as needed in the case of PIXE analysis, results in a degradation of the beam spatial resolution. The attainable image contrast both in off-axis and in on/off-axis STIM is hampered by this fact. Furthermore, there is an inherent spectral degradation occurring in off-axis STIM as mentioned in the previous section thus producing a worse image contrast than in the case of on/off-axis STIM as can be verified in Fig. 2.

3.2. Detector damage and type

The different STIM experimental geometries imply different risks of detector damage and need for substitution. In the case of the off-axis or on/off-axis geometries, all the exposed active area of the particle detector is used to collect signals and then long time of operation is expected. When the detector is used at on-axis STIM geometry, it should be taken into account that the used active area of the detector is now of the same order of magnitude as the sample scan.

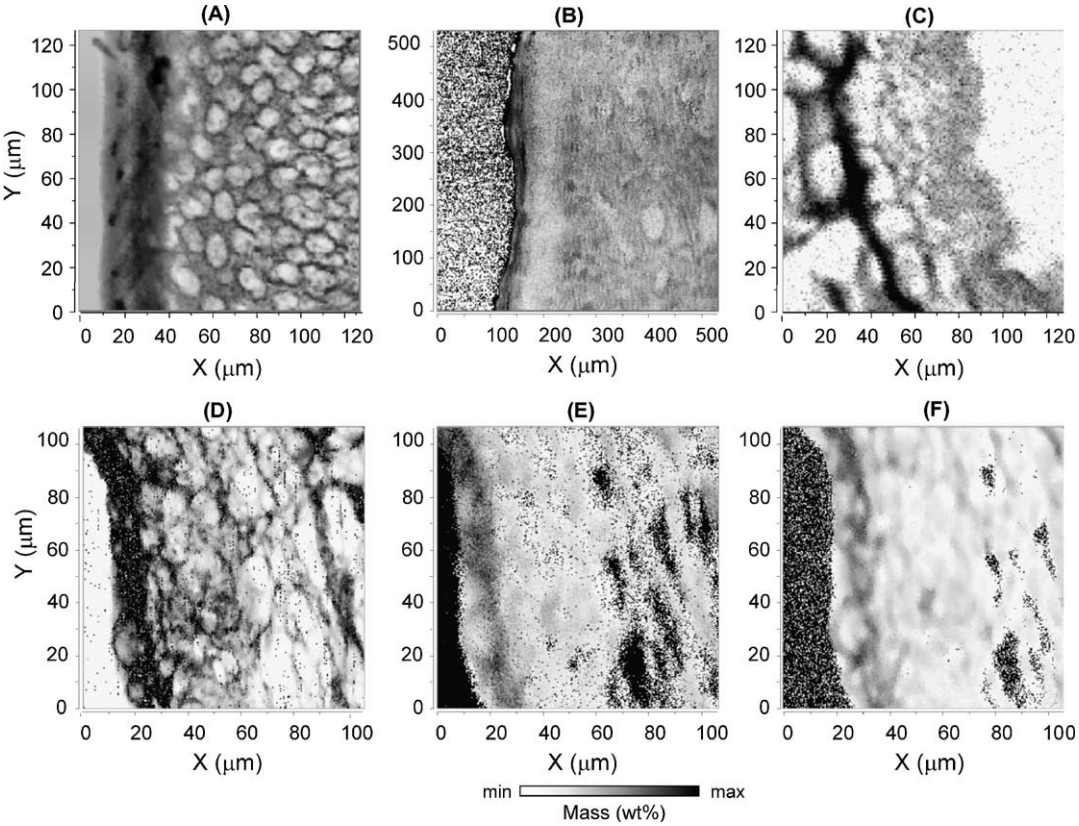

Fig. 2. Images obtained for on-axis STIM, off-axis STIM, and on/off-axis STIM geometries at different groups. (A) 14 μm section of mouse foot sole skin, on-axis STIM at Bordeaux; (B) 25 μm section of pig skin, off-axis STIM at Debrecen; (C) 14 μm section of pig skin, on/off-axis STIM at Lund; 14 μm section of pig skin, observed for the three STIM geometries (Lisbon); (D) on-axis; (E) off-axis and (F) on/off-axis.

At the Lisbon STIM set-up a PIN diode was directly irradiated with a 2 MeV proton beam with count rate close to 3000 ions/s for different scan amplitudes. The maps obtained (Fig. 3) show a degradation of the PIN diode after a scan of 26×26 μm^2 with a total amount of 1.5×10^6 particles entering the detector. Even for a scan of 212×212 μm^2, it is possible to recognize deterioration of a previous scan of 106×106 μm^2. The ion dose was similar although distributed on an area at least 16 times as big. The total STIM spectra obtained are also shown in Fig. 3 where the alteration in the detector response function can be observed. The listmode data collected for the 26×26 μm^2 scan allows to measure the pulse height variation rate, that was found to be of 1.7 keV/10^5 ions. This variation rate is similar to the one found by Maetz et al. [8] for a PIPS detector located at 55 mm from the image plane and irradiated with a 0.5 μm^2 focused proton beam. Taking into account parameters as the beam angle divergence, microprobe demagnification coefficients and distance between detector and sample at the Lisbon set-up, calculations lead to a pulse height variation of 4.0 keV/(200 protons/μm^2). This result is compatible with the one found in the work of Simons et al. [9]. In that work it is shown that when scanning a PIPS detector with 4 MeV He^+ ions, with the detector located at the beam focal plane, there is a shift on the energy pulse height of 4.16 keV per 1×10^{10} ions/cm^2.

These observations imply that an on-axis STIM analysis with a scan inferior to 100×100 μm^2 must be performed with extra care at the expense of

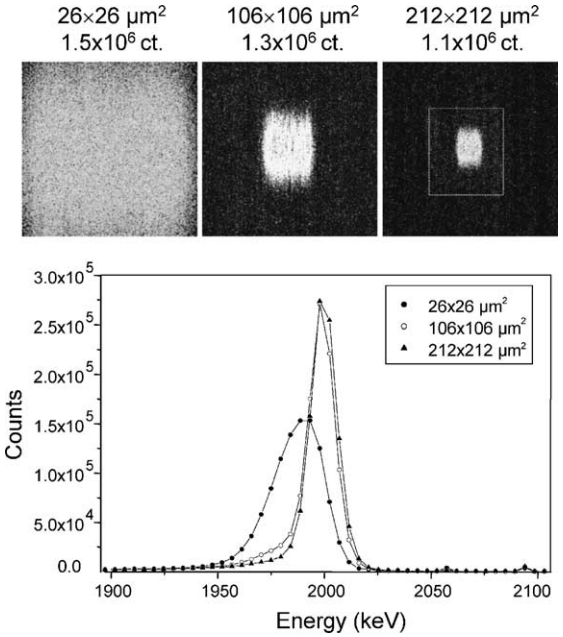

Fig. 3. Results of a direct irradiation with a 2.0 MeV proton beam of a PIN diode located at 40 mm from the focal plane after three consecutive beam scan amplitudes. The induced detector beam damage as well as the alteration in the detector response function are shown.

getting a highly damaged detector area and then a misleading image contrast (Fig. 4).

According to previous work [8,9] and to results obtained with the set-ups used in this work, the radiation damage in a Si PIN diode or in a PIPS detector should be of the same order of magnitude although the higher reverse bias used in a PIPS can slightly improve the charge collection efficiency by reducing trapping and recombination of the charge carriers. As the signal in an undamaged part of the detector is not too much dependent on contiguous damaged detector zones [8], a set-up capable of changing detector position could also be advantageous.

As sample thickness resolution is a function of detector resolution [10], the choice of detector type may play a role in the image quality obtained in a STIM experiment. However, the Si PIN diode used presents a resolution of 15 keV and differences may only be expected for a very high quality (FWHM better than 10 keV) PIPS detector.

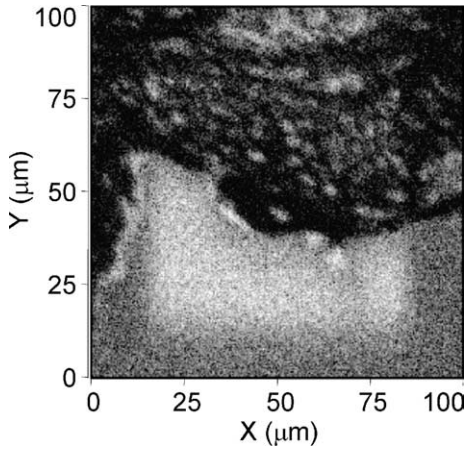

Fig. 4. On-axis STIM image of skin sample obtained during a 150×150 μm^2 scan where a previous scan of 100×100 μm^2 was performed. The PIPS detector damage area can be identified.

3.3. Data reduction

The spectral information gathered during the analysis can be reduced off-line into a single map when all the events are recorded in an "event-by-event mode". The single map is obtained from statistical data treatment of the events occurring at each pixel. This can be carried out directly with the OMDAQ computer code [11] as it is done by the Lisbon group or through algorithms developed at each of the laboratories. At Debrecen, the extraction of the pixel information (i.e. mean energy and mean energy-loss values) from the OMDAQ "event by event" file and the imaging is done with a new software package developed for true elemental mapping purposes [12]. Bordeaux group developed an acquisition and data treatment system [3], including a routine for pixel statistics reduction using mean and median filtering of transmitted energy with imaging being performed by the Amira environment with different colour scale possibilities for increased contrast [13]. At Lund the KMAX data acquisition software produces average energy-loss maps. A user-written plug in to GeoPIXE [14] converts data into μg/cm^2 images. The maps obtained with median energy (whether transmitted or lost) show a better contrast than those obtained with the average energy due to a smaller influence of outlier values.

3.4. Modifications of skin samples

The modifications of biological materials occurring during PIXE analysis can be assessed by simultaneous collection of STIM data, if the information is recorded in event-by-event mode. Sample alterations can be estimated by sorting data at successive intervals of time. Mapping the information obtained with STIM off-axis geometry, the definition of details is often ambiguous due to the poor resolution achieved, contrasting with that obtained with the on/off-axis geometry. When the concentrations determined by PIXE have to be associated with specific tissue details, such as identification of cell layers of the stratified epidermis tissue, high precision in the definition of relative positions at the elemental map is required. The high resolution granted by STIM on/off-axis geometry may not be sufficient as sample contracts non-uniformly during analysis. This aspect may be minimized if the initial and the final conditions of the sample submitted to PIXE analysis could be assessed. STIM on-axis using very low currents that do not significantly affect the sample morphology can be used to record those stages. Besides the effective gain in resolution and consequently in sample morphology definition accomplished by STIM on-axis at limit stages of the overall analytical process, the sample modifications can be estimated and the position validation of elemental profiles obtained by PIXE can be achieved. If the quantitative information is gathered from a sequence of point analysis (roughly the beam area) selected after PIXE scan has been done, the final STIM image should reasonably reflect the sample condition in terms of morphology at the moment when point analysis was performed, what can additionally be confirmed by sorting last information recorded in event-by-event mode for the PIXE scan and comparing sample boundaries (or details) with those determined for the final STIM image.

The initial and final sample conditions, before and after PIXE irradiation, were compared and modifications estimated, as illustrated in Fig. 5. Variations observed in position coordinates of sample details by report to the initial coordinates set in the first map of on-axis STIM, were found to be of 15% that represents approximately 15 μm of section shrinkage for a scanned area of $106 \times 106\ \mu m^2$. Comparing the last 20% of events recorded during the PIXE scan with the final STIM image obtained, after a line of 10–15 point analysis had been done, variations in relative

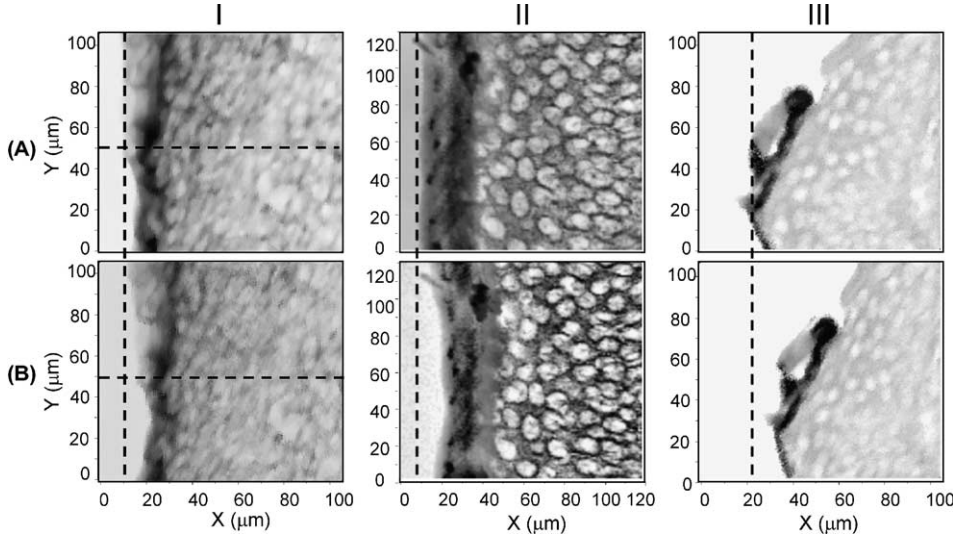

Fig. 5. Initial (A), and final (B), on-axis STIM images for of human skin (I), human skin grafted on SCID mouse skin (II), and pig skin (III) sections. The dashed cursor line indicates the initial section edge position.

coordinates of section details were found to be negligible.

Considering transversal 14 μm sections of different skin types (mouse, pig and human skin) the contraction of the stratified epidermis observed, preferentially occurred in the direction of the outer layers to the inner layers of skin. However, these modifications could not be associated to skin type, current applied (100–400 pA), amplitude of scan (50–100 μm^2) or areal density (300–1000 $\mu g/cm^2$) of the section inspected. Even for scans of sections of the same material results can differ (Fig. 6).

The sample contraction is accompanied by mass loss that can be verified through the width variation of the STIM (off-axis or on/off-axis geometries) spectra along the irradiation. From the quantitative analysis point of view, the mass loss can be accounted through the RBS or the STIM spectral information recorded simultaneously to PIXE spectra.

Thus, point analysis coordinates can be overlapped to the STIM on-axis image taken after total PIXE analysis has been carried out. The elemental profiles obtained can then be matched with morphology.

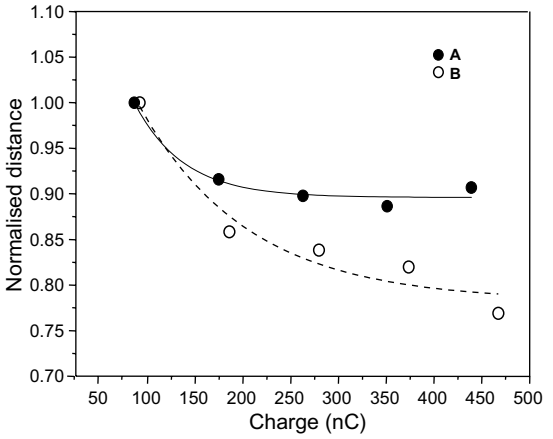

Fig. 6. Shrinkage (arbitrary units) observed for two scanned areas of 106×106 μm^2 (A and B) of 14 μm sections of human skin, versus accumulated charge. The mean current used in each scan was of 400 pA. Distance between two sample details in sequential PIXE scans was normalised to the first PIXE scan recorded. Last position was determined through STIM on-axis image. The lines (solid and dashed) represent the exponential fit for each set of points.

4. Conclusions

The purpose of using STIM technique in three different geometries was to compare its performance in assessing sample structure identification and the modifications of biological thin specimens under usual PIXE analysis conditions in order to validate PIXE elemental distribution images and their ability to determine mass loss to be used in elemental quantification.

When simultaneous STIM and PIXE analysis are performed, STIM on/off-axis geometry grant better image resolution than the off-axis scheme. For STIM on-axis, the detector damage occurring during analysis should be taken into account, once a dose of only 200 ions/μm^2 induces a pulse height variation of 1–2 channels for spectra collected with a regular energy calibration of 2–4 keV/channel. The widening of the detector life span can be achieved if a system for changing detector position would be implemented. Due to the good energy resolution of PIN diode detectors, only very high-resolution PIPS detectors (FWHM<10 keV) are expected to contribute to better STIM image contrast. Statistical treatment of STIM data is useful in the morphology characterization of biological tissues. Applying median energy procedures to STIM data, usually gives good image contrast.

High quality skin mass density images were obtained with on-axis STIM after statistical data reduction, allowing precise identification of tissue morphologic details. This is of the utmost importance to identify cellular environments, such as the skin layers of the stratified epidermis tissue, enabling to correlate elemental profiles with morphology. During PIXE analysis, skin shrinkage that can be of the order of 15% occurs, thus compromising the initial structure identification. It is recommended that after obtaining the PIXE elemental distribution maps and selecting a region of interest, the concentration profiles should be determined by several point analysis and mass normalization done with the simultaneous acquired RBS or STIM (off-axis or on/off-axis) spectra.

Precise location of the analysed spots can be done by a final on-axis STIM image.

Acknowledgement

This work was partially supported by the EC/QLK4-CT-2002-02678 contract. Support from the Hungarian Research Found (OTKA) under contract Nos. A 080, M 041939, M 36324 is gratefully acknowledged.

References

[1] Y. Matsumura, H.N. Ananthaswamy, Toxicol, Appl. Pharmacol. 195 (2004) 298.
[2] J. Schulz, H. Hohenberg, F. Pflucker, E. Gartner, T. Will, S. Pfeiffer, R. Wepf, V. Wendel, H. Gers-Barlag, K.-P. Wittern, Adv. Drug Delievery Rev. 54 (2002) S157.
[3] Deves, Ortega, Anal. Bioanal. Chem. 374 (2002) 390.
[4] Zs. Kertész, Z. Szikszai, I. Uzonyi, A. Simon, Á.Z. Kiss, Nucl. Instr. and Meth. B, these Proceedings, doi:10.1016/j.nimb.2005.01.042.
[5] L.C. Alves, M.B.H. Breese, E. Alves, A. Paúl, M.R. da Silva, M.F. da Silva, J.C. Soares, Nucl. Instr. and Meth. B 161–163 (2000) 334.
[6] J. Pallon, Nucl. Instr. and Meth. B 22 (1987) 87.
[7] J. Pallon, V. Auzelite, M. Elfman, M. Garmer, P. Kristensson, K. Malmqvist, C. Nilsson, A. Shariff, M. Wegdén, Nucl. Instr. and Meth. B 219–220 (2004) 988.
[8] M. Maetz, W.J. Przybylowicz, J. Mesjasz-Przybylowicz, A. Schubler, K. Traxel, Nucl. Instr. and Meth. B 158 (1999) 292.
[9] D.P.L. Simons, A.J.H. Maas, P.H.A. Mutsaers, M.J.A. de Voight, Nucl. Instr. and Meth. B 130 (1997) 160.
[10] M.B.H. Breese, D.N. Jamieson, P.J.C. King, Materials Analysis Using a Nuclear Microprobe, John Wiley & Sons, New York, 1996.
[11] G.W. Grime, M. Dawson, Nucl. Instr. and Meth. B 104 (1995) 107.
[12] I. Uzonyi, Gy, Szabó, Nucl. Instr. and Meth. B, these Proceedings, doi:10.1016/j.nimb.2005.01.050.
[13] http://www.tgs.com/support/amira_doc/index.htm.
[14] C.G. Ryan, D.R. Cousens, GeoPIXEII, CSIRO. Available from <http://nmp.csiro.au>.